

# REPORT DOCUMENTATION PAGE

Form Approved  
OMB No. 0704-0188

Public reporting burden for this collection of information is estimated to average 1 hour per response, including the time for reviewing instructions, searching existing data sources, gathering and maintaining the data needed, and completing and reviewing this collection of information. Send comments regarding this burden estimate or any other aspect of this collection of information, including suggestions for reducing this burden to Department of Defense, Washington Headquarters Services, Directorate for Information Operations and Reports (0704-0188), 1215 Jefferson Davis Highway, Suite 1204, Arlington, VA 22202-4302. Respondents should be aware that notwithstanding any other provision of law, no person shall be subject to any penalty for failing to comply with a collection of information if it does not display a currently valid OMB control number. PLEASE DO NOT RETURN YOUR FORM TO THE ABOVE ADDRESS.

1. REPORT DATE (DD-MM-YYYY) 15-10-2007		2. REPORT TYPE final report		3. DATES COVERED (From - To) Aug 01, 2005 - July 31, 2007	
4. TITLE AND SUBTITLE Fueling and stabilizing a biomolecular motor-powered biosensor for remote detection scenarios				5a. CONTRACT NUMBER	
				5b. GRANT NUMBER FA9550-05-1-366	
				5c. PROGRAM ELEMENT NUMBER	
6. AUTHOR(S) Henry Hess (Principal Investigator)  hhess@mse.ufl.edu				5d. PROJECT NUMBER	
				5e. TASK NUMBER	
				5f. WORK UNIT NUMBER	
7. PERFORMING ORGANIZATION NAME(S) AND ADDRESS(ES)  University of Florida Awards Administration Office 207 Grinter Hall, POB 115500 Phone: 352-392-5991 Fax: 352-392-4522				8. PERFORMING ORGANIZATION REPORT NUMBER	
9. SPONSORING / MONITORING AGENCY NAME(S) AND ADDRESS(ES) USAF, AFRL AF Office of Scientific Resea 875 N. Randolph Str. RM 3112 Arlington, VA 22203 Valarie I. Hall 703-696-9736				10. SPONSOR/MONITOR'S ACRONYM(S)  N/Defense Advanced Research Projects Agency (DARPA)	
				11. SPONSOR/MONITOR'S REPORT NUMBER(S)	
12. DISTRIBUTION / AVAILABILITY STATEMENT  Approved for public release. Distribution is unlimited.				AFRL-SR-AR-TR-07-0464	
13. SUPPLEMENTARY NOTES  Program Manager: Dr. Hugh DeLong, AFOSR/NL, (703) 696-7722, hugh.delong@afosr.af.mil					
14. ABSTRACT The overall goal of this collaborative project (partners: Sandia National Lab, Naval Research Lab, ETH Zurich, AECOM New York) is to demonstrate a biomolecular motor-powered "smart dust" biosensor, which can be read-out remotely in a standoff detection scenario. The contribution of the U. of Florida team centered on (1) developing methods to stabilize biosensor performance against fluctuations in temperature and light exposure and (2) testing the performance of fluorescent tags and complete biosensors. Significant additional effort has been expended in developing a design and fabrication procedure for a prototype of the biomolecular motor-powered biosensors, which currently constitutes the showstopper in this collaborative project. This critical effort has yielded an initial demonstration of the sensor concept.					
<h1>20071101405</h1>					
15. SUBJECT TERMS					
16. SECURITY CLASSIFICATION OF:			17. LIMITATION OF ABSTRACT	18. NUMBER OF PAGES	19a. NAME OF RESPONSIBLE PERSON
a. REPORT	b. ABSTRACT	c. THIS PAGE			19b. TELEPHONE NUMBER (include area code)

**Objectives:** No changes.

**Status of effort:**

All related research projects have been completed and manuscripts describing the achieved advances are currently under consideration or in the process of being submitted. The next steps in designing and fabricating a biomolecular motor-powered biosensor are being taken in FY08 with support from the Office of Naval Research (N00014-07-1-0982).

The "Comprehensive technical summary" section will describe the detailed results of the following subprojects:

- (A) Temperature stabilization of biomolecular motor-powered devices
- (B) Absolute and relative brightness of nanoscale optical tags for remote detection
- (C) Velocity optimization for pick-up of optical tags by molecular shuttles
- (D) Proof-of-principle demonstration of basic biomolecular motor-powered sensor

**Accomplishments/Highlights:**

**H. Hess: "Biomolecular motor-powered devices", Science 312, 861 (2006), invited perspective**

T. Nitta, A. Tanahashi, M. Hirano, H. Hess: "Simulating molecular shuttle movements: Towards computer-aided design of nanoscale transport systems", Lab on a Chip 6(7), 881-885 (2006)

R. Seetharam, Y. Wada, S. Ramachandran, H. Hess, P. Satir: "Long-term storage of bionanodevices by freezing and lyophilization", Lab on a Chip, 6, 1239-1242 (2006)

T. Fischer, H. Hess: "Materials chemistry challenges in the design of hybrid bionanodevices: Supporting protein function within artificial environments", J. Mater. Chem., 2007, 17, 943 – 951

P. Katira, A. Agarwal, T. Fischer, H.-Y. Chen, X. Jiang, J. Lahann, H Hess: "Quantifying the performance of protein-resisting surfaces at ultra-low protein coverages using kinesin motor proteins as probes", Advanced Materials, in print

**The next phase of the project is currently supported by the "University of Florida Center for Sensor Technologies and Materials" funded by the Office of Naval Research (N00014-07-1-0982).**

**Personnel Supported:**

Henry Hess, PhD (PI) – Assistant Professor  
Thorsten Fischer, PhD – postdoctoral researcher  
Robert Tucker – graduate student  
Isaac Luria – graduate student  
Ashutosh Agarwal – graduate student  
Parag Katira – graduate student  
Isaac Finger – graduate student  
Elizabeth Mobley – undergraduate researcher

**Interactions:** Oral presentations:

H. Hess: "Biomolecular Motors: Engines for Nanotechnology", Seminar of the Department of Pharmacology, University of California, Los Angeles, CA (2005), invited

H. Hess: "Biomolecular Motors: Engines for Nanotechnology", Seminar of the BioSecurity & NanoSciences Laboratory and the Center For Micro and Nano Technology, Lawrence Livermore National Laboratory, CA (2005), invited

H. Hess: "Biomolecular Motors: Engines for Nanotechnology", Seminar of the Materials Science and Engineering Department, University of Michigan, MI (2005), invited

H. Hess: "Biomolecular Motors: Engines for Nanotechnology", Geometry, Graphics, Vision, Visualization/Visual Simulation (G2V2) Seminar, Department of Computer and Information Science and Engineering, University of Florida, FL (2006), invited

H. Hess: "Filming the actions of bionanomotors with epi-fluorescence microscopy", 2006 Annual Joint Symposium, Florida Chapter of the AVS and Florida Society for Microscopy, Orlando, FL, (2006), invited

H. Hess: "From Molecular Robotics to Active Self-assembly: Biomolecular Motors do the Job", Symposium AA, 2006 MRS Spring Meeting, San Francisco, CA (2006), invited

H. Hess: "On Biomolecular Motors", NSF Center for Molecular Cybernetics PI meeting 5/17/06, Ann Arbor, MI (2006), invited

H. Hess: "Biomolecular motors for directed assembly and hybrid devices", Gordon Conference for Nanostructure Fabrication, Tilton, NH (7/17/2006), invited

H. Hess, A. Agarwal, T. Fischer, P. Katira, M. Kinahan, I.T. Luria, R. Tucker: "Applications of Biomolecular Motors in Nanotechnology", ACS Annual Meeting, San Francisco, CA (9/14/2006), invited

H. Hess: "Biomolecular motors for directed assembly and hybrid devices", Seminar of the College of Nanoscale Science and Engineering, SUNY Albany, NY (10/27/2006), invited

T. Fischer, A. Agarwal, P. Katira, I. Luria and H. Hess: "Biomolecular Motors - The Natural Way of Active Transport in Nanofluidic Devices" MRS Fall Meeting, Boston, MA (11/30/2006)

H. Hess, A. Agarwal, T. Fischer, P. Katira, M. Kinahan, I.T. Luria, R. Tucker: "Applications of Biomolecular Motors in Nanotechnology", AIChE Annual Meeting, San Francisco, CA (11/15/2006), invited

H. Hess: "Nanoscale Transport Systems Based on Molecular Shuttles", Ladenburger Discourse meeting on "From Bio-Inspired Logistics to Logistics-Inspired Bio-Nano-Engineering" organized by the Gottlieb Daimler and Karl Benz Foundation, Ladenburg, Germany (4/4/2007), invited

H. Hess: "Biomolecular motors for directed assembly and hybrid devices", Seminar of the Chemistry Division, Argonne National Lab, Chicago, IL (4/30/2007), invited

H. Hess: "Biomolecular motors for directed assembly and hybrid devices", Seminar of the Department for Chemistry and Biomedical Sciences, University of Kalmar, Kalmar, Sweden (5/10/2007), invited

H. Hess: "Applications of Biomolecular Motors in Microfluidic Devices", Gordon Conference of Physics & Chemistry of Microfluidics, Waterville, NH (7/16/07), invited

**Discoveries, inventions, patent disclosures:** None

**Honors/Awards:** Thorsten Fischer (postdoctoral researcher) received a Feodor Lynen postdoctoral fellowship from the Alexander-von-Humboldt foundation partially supporting his project-related research (2006).

## Comprehensive technical summary of significant work accomplished:

In a collaboration with Sandia National Lab (G. Bachand), the Naval Research Lab (B. Ratna), the Albert Einstein Medical College (P. Satir) and the Swiss Federal Institute of Technology (V. Vogel) and with funding from the DARPA-DSO Biomolecular motors program we are designing a “smart dust” type biosensor powered by biomolecular motors (Fig. 1).

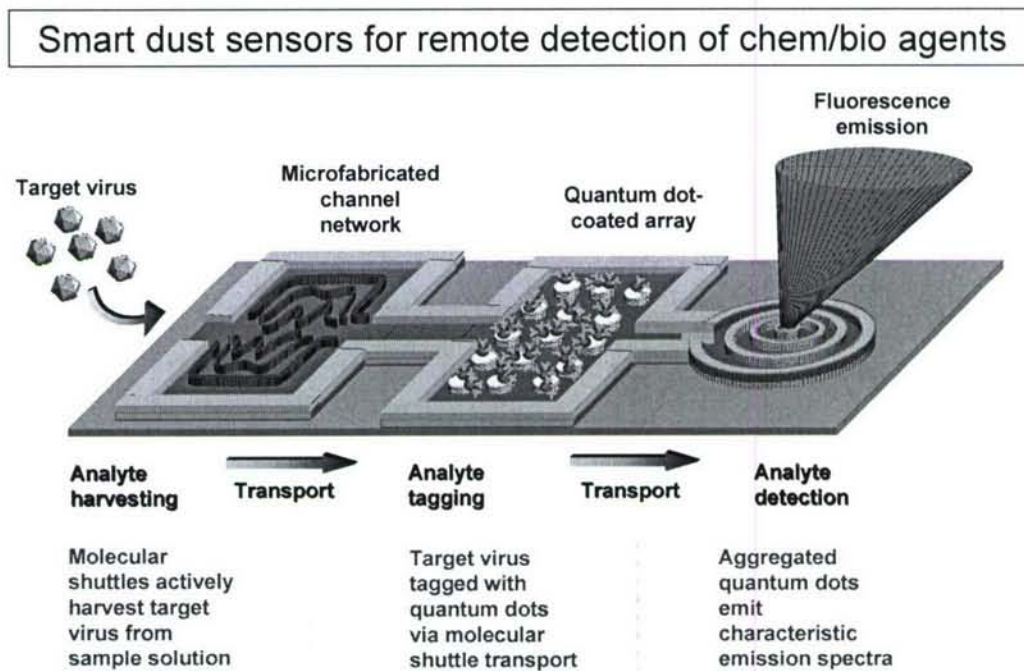


Figure 1: The schematic design of a “smart dust” biosensor, where transport of antibody-functionalized microtubules is driven by biomolecular motors. The microtubules capture target chem/bio agents, transport them to a second chamber for tagging, and transfer the targets and tags to a third chamber. In the third chamber, the presence of optical tags is detected remotely by fluorescence measurements.

Here, the detailed results of the following subprojects will be described:

- (A) Temperature stabilization of biomolecular motor-powered devices
- (B) Absolute and relative brightness of nanoscale optical tags for remote detection
- (C) Velocity optimization for pick-up of optical tags by molecular shuttles
- (D) Proof-of-principle demonstration of basic biomolecular motor-powered sensor

In combination, these results present a significant advance towards the goal of fabricating a biomolecular motor-powered “smart dust” sensor. It has to be emphasized, that the developed solutions to temperature stabilization, velocity optimization, and controlled activation via caged ATP reinforce each other by working in concert. For example, a reduction in ATP concentration to reduce temperature dependence is also desirable to optimize the shuttle velocity for pick-up of optical tags. Similarly, the reduced ATP concentration is more readily attainable by photolytic release of caged ATP in the solution.

## (A) Temperature stabilization of biomolecular motor-powered devices

**Abstract:** Autonomous micro- and nanodevices, such as “smart dust”, operate in environments with variable temperatures. The activity of integrated biological components, such as enzymes, typically exhibits a pronounced dependence on temperature. Here, strategies to minimize the influence of temperature on device performance are discussed. The temperature dependence of the Michaelis-Menten parameters  $v_{\max}$  and  $K_m$  is measured for kinesin motor proteins, and it is concluded that for molecular shuttles powered by kinesin motors a range of subsaturating substrate concentrations exists at which the increase of maximal activity of the kinesin motor with increasing temperature is almost cancelled by a decreasing affinity to its substrate. This example illustrates that temperature stabilization and high activation are competing goals.

**Introduction:** A paradigm shift in lab-on-a-chip devices from microfluidic cartridges utilized by desktop or handheld devices to “smart dust”, submillimeter-sized devices for remote detection<sup>2,3</sup> requires a level of miniaturization and integration only known from biological systems. A promising route towards developing highly functional “smart dust” prototypes is the design of hybrid devices, which integrate biological nanomachines into a microfabricated synthetic structure.

One of the challenges arising from this hybrid approach is the stabilization of device operation against temperature changes. The activity of biological nanomachines, such as enzymes, is strongly temperature-dependent, typically doubling for every 10 °C increase in temperature at saturating substrate concentrations. Traditionally, temperature can be and is closely controlled in biotechnological processes and microfluidic devices<sup>4-6</sup>, either to maintain a stable activity or to switch between active and inactive states of the system. In a “smart dust” device, active control of temperature is not feasible due to the rapid heat exchange with the environment and the high complexity of the system, requiring energy storage and conversion and a control mechanism. Instead, internal processes have to be stabilized against temperature fluctuations. Inspiration for stabilization strategies is provided by poikilotherm organisms, who compensate for temperature changes on a wide range of timescales<sup>7,8</sup>.

Two biological strategies providing instantaneous compensation are of particular interest. On one hand, metabolic networks can display temperature compensation due to the existence of feedback loops<sup>9</sup>. The engineering equivalent is found in the canonical layout for temperature-compensated electronic circuits<sup>10</sup>. On the other hand, enzymes themselves can display near constant activity for subsaturating substrate concentrations in a limited temperature range. An example is lactate dehydrogenase from Alaskan king crab, whose  $K_m$  value increases with temperature and compensates for the increasing  $v_{\max}$  value<sup>11</sup>. From an engineering point of view, this approach, preferable due to its simplicity, is similar to employing a material with intrinsic temperature compensation such as INVAR steel<sup>12</sup>.

Here, the temperature dependence of kinesin motor protein activity is determined at saturating and for the first time subsaturating substrate concentrations, and the implications for the design of kinesin motor powered hybrid devices are discussed.

Kinesin and other motor proteins have evolved in nature to provide actuation and transport within cells<sup>13,14</sup>. Recently, motor proteins and their associated filaments (microtubules in the case of kinesin) have been employed for the transport of nanoscale cargo in microfabricated structures<sup>15-23</sup>, and it has been shown that these “molecular shuttle” systems<sup>24,25</sup> can be applied to tasks such as force measurements<sup>26</sup>, surface imaging<sup>27</sup>, single molecule manipulation<sup>28</sup>, computing<sup>29</sup> and biosensing<sup>30,31</sup>. As a result, kinesin motors are likely to be integrated in future “smart dust” devices to provide active transport, complementing pressure-driven fluid flow and electroosmotic flow<sup>32</sup>.

**Methods:** *Kinesin and microtubule preparation:* A kinesin construct consisting of the wild-type, full-length *Drosophila melanogaster* kinesin heavy chain and a C-terminal His-tag was expressed in *Escherichia coli* and purified using a Ni-NTA column.<sup>33</sup> Rhodamine-labeled tubulin (3.2 mg/mL, Cytoskeleton, Denver, CO) was polymerized at 37 °C for 30 min in BRB80 buffer (80 mM PIPES, 1 mM EGTA, 2 mM MgCl<sub>2</sub>, pH 6.9) with 1 mM GTP, 4 mM MgCl<sub>2</sub>, and 5% DMSO, and subsequently diluted 100-fold into BRB80 with 10 μM paclitaxel. *Variable temperature motility assay:* A new flow cell was assembled from a square coverslip (22×22 mm), double-sided tape as spacer, and a circular coverslip (15 mm diameter) for each set of measurements at a given

ATP concentration. The inner surfaces of the flow cell were coated with casein (0.4 mg/ml in BRB80 for 5 min) and kinesin (10 nM in BRB80 with 0.1 mg/ml casein and the desired ATP concentration for 5 min). A motility solution containing 3.2  $\mu\text{g}/\text{mL}$  microtubules, ATP (1000  $\mu\text{M}$ , 200  $\mu\text{M}$ , 100  $\mu\text{M}$ , 50  $\mu\text{M}$ , 25  $\mu\text{M}$  or 10  $\mu\text{M}$ ), casein (0.1 mg/ml), and an antifade solution (20 mM D-glucose, 20  $\mu\text{g}/\text{mL}$  glucose oxidase, 8  $\mu\text{g}/\text{mL}$  catalase, 1% dithiothreitol) was introduced and the edges of the coverslips were sealed with Apiezon<sup>®</sup> grease to minimize evaporation. The flow cell was placed upside down in a stage heater (Model RC-20, Warner Instruments Inc.), the top (square) cover slip was coated with silver paste and covered with an aluminum plate, and the top fasteners of the stage heater were tightened. Heat is transferred through the aluminum plate to the top cover slip and through the stage heater to the bottom coverslip from a pair of 20  $\Omega$  resistors heated by an automatic temperature controller (Warner Instruments Inc., TC-324B). The microscope objective (Nikon 100 X oil) was heated by a resistive wire (Nichrome 60, Pelican Wire Co.) powered with a DC regulated power supply (EXTECH<sup>®</sup> instruments). The power supply was manually regulated to heat the objective to the same temperature as the flow cell.

**Measurement of temperature:** The thermistor from the automatic temperature controller was connected to the stage heater near the flow cell. A second thermocouple was attached to the objective and read using a multimeter. Thermocouple readings in the temperature range of interest were calibrated against an alcohol thermometer.

**Measurement of velocity:** An Eclipse TE2000-U fluorescence microscope (Nikon, Melville, NY) with a 100X oil objective (N.A. 1.4), an X-cite 120 lamp (EXFO, Ontario, Canada), a rhodamine filter cube (#48002, Chroma Technologies, Rockingham, VT) and an iXon EMCCD camera (ANDOR, South Windsor, CT) and were used to image microtubules on the bottom surface of flow cells. From a flow cell with a specific ATP concentration a set of 10 images were taken in 5 second intervals for each one of seven temperatures (22, 25, 28, 31, 34, 37, 40  $^{\circ}\text{C}$ ). The experiment was begun at room temperature and the flow cell was slowly heated until microtubules disintegrated and motility stopped. In each set of images five microtubules were tracked manually over 5 frames, and a mean velocity was calculated with an error of <3%.

**Results:** The velocity measurements (Fig. 1) show the expected Arrhenius-type increase with increasing temperature for a saturating ATP concentration (1 mM), while the velocity is nearly independent of temperature for ATP concentrations of less than 25  $\mu\text{M}$ . For comparison, the data of Kawaguchi and Ishiwata<sup>34</sup> for saturating ATP concentrations (1 mM) obtained with bovine kinesin are included. Here, kinesin from *drosophila* was utilized which may account for the 30% lower velocities.

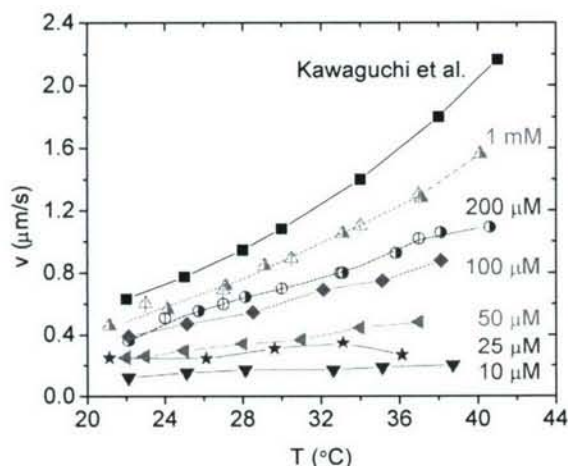


Figure 1: Microtubule gliding velocity as function of temperature for various ATP concentrations. Black squares are the data published by Kawaguchi and Ishiwata<sup>34</sup> for 1 mM ATP.

A plot of velocity as function of ATP concentration for a series of temperatures (Fig. 2) was obtained by interpolating the data points in Fig. 1 for six temperatures. Fitting these curves with a Michaelis-Menten equation  $v([\text{ATP}], T) = v_{\text{max}}(T) \times [\text{ATP}] / (K_m(T) + [\text{ATP}])$  revealed the temperature dependence of the velocity at saturating substrate concentrations  $v_{\text{max}}$  and the Michaelis constant  $K_m$  (Fig. 3).

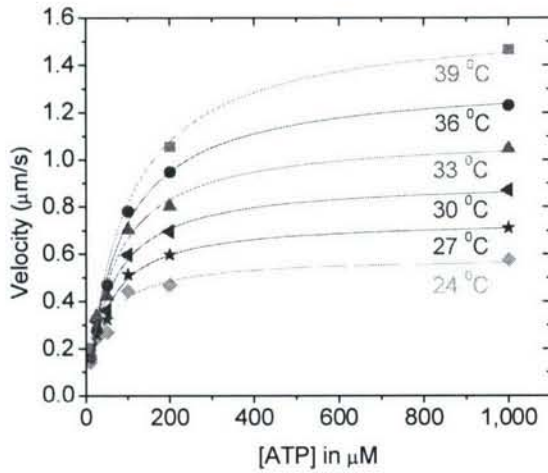


Figure 2: Microtubule gliding velocity as function of ATP concentration for a series of temperatures obtained by interpolating the data presented in Fig. 1. Lines are fits to Michaelis-Menten functions with  $v_{\max}$  and  $K_m$  as parameters.

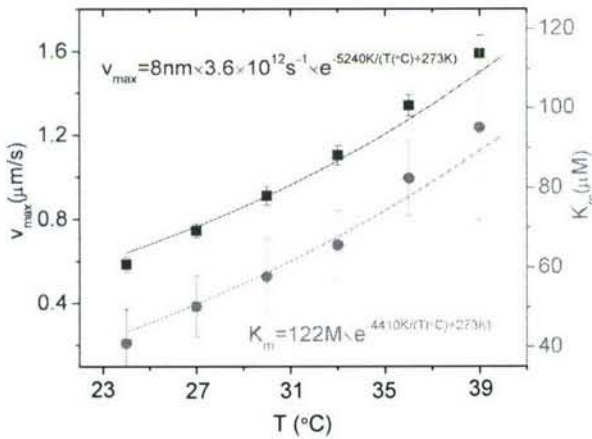


Figure 3: Maximal velocity  $v_{\max}$  (blue squares) and  $K_m$  (red circles) as function of temperature.

Böhm et al.<sup>35</sup> reported that the  $K_m$  values for porcine kinesin at temperatures of 25 °C and 35 °C to be 66±/−10 μM and 79±/−8 μM, which is in reasonable agreement with our measurements (Fig. 3).

The temperature-dependent  $v_{\max}$  and  $K_m$  parameters were graphed in Arrhenius plots  $\ln(v_{\max})=f(1/T)$ ,  $\ln(K_m)=g(1/T)$  and the activation energies were determined by linear error-weighted least-square fits to be 44 kJ/mol (18  $k_bT$ ) and 37 kJ/mol (15  $k_bT$ ) for  $v_{\max}$  and  $K_m$ , respectively. Of course, the fitted “activation energy” related to  $K_m=(k_{-1}+k_2)/k_1$  does not represent an actual energy barrier but is a function of the whole potential energy surface of the enzymatic reaction and is dominated by the free energy change occurring upon ATP binding.

**Discussion:** The sensitivity of an enzymatic reaction is conveniently framed in terms of the  $Q_{10}$  value, defined as the ratio of turnover rates at a 10 °C increased temperature and the reference temperature. Complete temperature compensation is achieved for a  $Q_{10}$  value of one. At saturating substrate concentrations the  $Q_{10}$  of an enzyme with a typical activation energy of 50 kJ/mol is close to two. However, for ATP concentrations much smaller than  $K_m$ , the  $Q_{10}$  value is given by:

$$Q_{10} = \frac{v_{\max}(T+10K) \times K_m(T)}{v_{\max}(T) \times K_m(T+10K)}$$

$$Q_{10} = \exp\left[\frac{E_A^v - E_A^K}{k_b T(T/10K + 1)}\right] \approx 1 + \frac{E_A^v - E_A^K}{30k_b T}$$

where  $E_A^v$  is the activation energy for rate determining step and  $E_A^K$  is the “activation energy” derived from the temperature dependence of  $K_m$ . In the present case, the  $Q_{10}$  at subsaturating ATP concentrations can be as small as 1.1, which means that the sensitivity of the system to temperature changes is ten-fold reduced.

The dependence of  $Q_{10}$  on ATP concentration is shown in Fig. 4, suggesting that for substrate concentration up to 10% of  $K_m$  the stabilization of the system is close to the optimum achievable by reducing the substrate concentration.

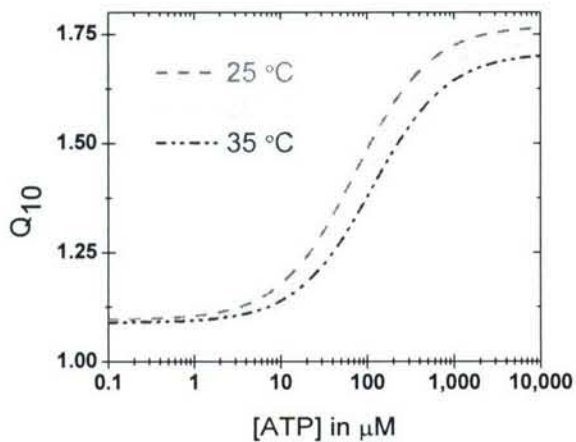


Figure 4:  $Q_{10}$  as a function of the ATP concentration at specific temperatures calculated from the fits shown in Fig. 3.

Rivera et al. suggested that due to its increased temperature stability and faster gliding velocities a kinesin-3 from *Thermomyces lanuginosus* is an attractive alternative to *drosophila* kinesin-1 in motor-driven nanobiodevices and characterized its temperature-dependent properties in detail.<sup>36</sup> For *Thermomyces* kinesin, the activation energy has been given by Rivera et al. as  $94 \pm 9$  kJ/mol (38 kT), and the  $K_m$  increased from  $42 \pm 7$   $\mu$ M at 25 °C to  $1.6 \pm 0.3$  mM at 50 °C leading to an estimate of  $E_A^k = 116 \pm 40$  kJ/mol (47 kT). At near zero ATP concentrations the  $Q_{10}$  is 0.7 and thus the *Thermomyces* kinesin activity falls with increasing temperature. At ATP concentrations of  $\sim 10$   $\mu$ M the activity changes only by 20 % in the range of 20 °C to 40 °C reaching a maximum at 25 °C, and at higher ATP concentrations the activity rises quickly with temperature and reaches a  $Q_{10}$  of more than 3.

**Conclusions:** The example of kinesin motor proteins, which are central in a number of nanobiodevices currently under development, illustrates that temperature stabilization of enzyme activity can be achieved at the expense of enzyme turnover by reducing the substrate concentration substantially if the Michaelis constant and the maximum turnover rate both increase with temperature. While complete temperature stabilization in general may require the design of a suitable enzymatic network, a reduction in substrate concentration is a straightforward approach with substantial benefit.

#### References:

1. M. J. Sailor and J. R. Link, *Chemical Communications*, 2005, 1375-1383.
2. T. A. Schmedake, F. Cunin, J. R. Link and M. J. Sailor, *Advanced Materials*, 2002, **14**, 1270-1272.
3. J. M. Kahn, R. H. Katz and K. S. J. Pister, *Journal of Communications and Networks*, 2000, **2**, 188-196.
4. D. L. Huber, R. P. Manginell, M. A. Samara, B. I. Kim and B. C. Bunker, *Science*, 2003, **301**, 352-354.
5. R. M. Guijt, A. Dodge, G. W. K. van Dedem, N. F. de Rooij and E. Verpoorte, *Lab on a Chip*, 2003, **3**, 1-4.
6. G. Mihajlovic, N. M. Brunet, J. Trbovic, P. Xiong, S. von Molnar and P. B. Chase, *Applied Physics Letters*, 2004, **85**, 1060-1062.
7. J. R. Hazel and C. L. Prosser, *Physiological Reviews*, 1974, **54**, 620-677.
8. G. N. Somero, *Annual Review of Ecology and Systematics*, 1978, **9**, 1-29.
9. P. Ruoff, M. Zakhartsev and H. V. Westerhoff, *Febs Journal*, 2007, **274**, 940-950.
10. P. Horowitz and W. Hill, *The art of electronics*, Cambridge University Press, Cambridge, 1989.
11. G. N. Somero, *Biochemical Journal*, 1969, **114**, 237-&.
12. M. van Schilfgaarde, I. A. Abrikosov and B. Johansson, *Nature*, 1999, **400**, 46-49.
13. M. Schliwa and G. Woehlke, *Nature*, 2003, **422**, 759-765.
14. J. Howard, *Mechanics of Motor Proteins and the Cytoskeleton*, Sinauer, Sunderland, MA, 2001.
15. D. V. Nicolau, H. Suzuki, S. Mashiko, T. Taguchi and S. Yoshikawa, *Biophys J*, 1999, **77**, 1126-1134.

16. Y. Hiratsuka, T. Tada, K. Oiwa, T. Kanayama and T. Q. Uyeda, *Biophys J*, 2001, **81**, 1555-1561.
17. P. Stracke, K. J. Böhm, J. Burgold, H. J. Schacht and E. Unger, *Nanotechnology*, 2000, **11**, 52-56.
18. M. G. L. van den Heuvel, C. T. Butcher, S. G. Lemay, S. Diez and C. Dekker, *Nano Letters*, 2005, **5**, 235-241.
19. R. Yokokawa, S. Takeuchi, T. Kon, M. Nishiura, R. Ohkura, K. Sutoh and H. Fujita, *Journal of Microelectromechanical Systems*, 2004, **13**, 612-619.
20. Y. Z. Du, Y. Hiratsuka, S. Taira, M. Eguchi, T. Q. P. Uyeda, N. Yumoto and M. Kodaka, *Chemical Communications*, 2005, **40**, 2080-2082.
21. Y. M. Huang, M. Uppalapati, W. O. Hancock and T. N. Jackson, *IEEE Transactions on Advanced Packaging*, 2005, **28**, 564-570.
22. S. G. Moorjani, L. Jia, T. N. Jackson and W. O. Hancock, *Nano Letters*, 2003, **3**, 633-637.
23. C.-T. Lin, M.-T. Kao, K. Kurabayashi and E. Meyhöfer, *Small*, 2006, **2**, 281-287.
24. J. R. Dennis, J. Howard and V. Vogel, *Nanotechnology*, 1999, **10**, 232-236.
25. H. Hess, J. Clemmens, D. Qin, J. Howard and V. Vogel, *Nano Letters*, 2001, **1**, 235-239.
26. H. Hess, J. Howard and V. Vogel, *Nano Letters*, 2002, **2**, 1113-1115.
27. H. Hess, J. Clemmens, J. Howard and V. Vogel, *Nano Letters*, 2002, **2**, 113-116.
28. C. Z. Dinu, J. Opitz, W. Pompe, J. Howard, M. Mertig and S. Diez, *Small*, 2006, **2**, 1090-1098.
29. D. V. Nicolau, D. V. Nicolau, G. Solana, K. L. Hanson, L. Filipponi, L. S. Wang and A. P. Lee, *Microelectronic Engineering*, 2006, **83**, 1582-1588.
30. G. D. Bachand, S. B. Rivera, A. Carroll-Portillo, H. Hess and M. Bachand, *Small*, 2006, **2**, 381-385.
31. S. Ramachandran, K.-H. Ernst, George D. Bachand, V. Vogel and H. Hess, *Small*, 2006, **2**, 330-334.
32. T. Nitta and H. Hess, *Nano Letters*, 2005, **5**, 1337-1342.
33. D. L. Coy, M. Wagenbach and J. Howard, *J Biol Chem*, 1999, **274**, 3667-3671.
34. K. Kawaguchi and S. Ishiwata, *Cell Motil Cytoskeleton*, 2001, **49**, 41-47.
35. K. J. Böhm, R. Stracke, M. Baum, M. Zieren and E. Unger, *FEBS Lett*, 2000, **466**, 59-62.
36. S. B. Rivera, S. J. Koch, J. M. Bauer, J. M. Edwards and G. D. Bachand, *Fungal Genetics and Biology*, In Press, Corrected Proof.

## (B) Absolute of nanoscale optical tags for remote detection

**Abstract:** The absolute brightness of fluorescent particles, such as dye-containing nano- and microspheres or quantum dots, is a critical design parameter for many applications relying on fluorescence detection. Measurements of the absolute brightness of a fluorescent microsphere are reported, and the implications for the design of kinesin motor protein-powered “smart dust” devices and the remote detection of fluorescence are discussed.

**Introduction:** The continuing miniaturization of lab-on-a-chip devices will eventually enable the transition from the typical creditcard-sized cartridge to “smart dust” devices<sup>1</sup> with submillimeter lateral dimensions. The feasibility and utility of such devices is illustrated by unicellular organisms, which can act as sensitive and highly integrated biosensors<sup>2</sup>. The aim of a collaborative research effort supported by the DARPA Biomolecular Motor Program is to design hybrid “smart dust” devices, where biomolecular motors power the active transport<sup>3,4</sup> of nanostructures capable of capturing analytes, labeling the captured analyte with fluorescent tags, and concentrating the analyte and tags in a specific area<sup>5-8</sup>. The analyte-dependent accumulation of fluorescent tags within optically transparent regions of the “smart dust” device can be detected remotely by fluorescence LIDAR, as demonstrated by Simonson et al. for fluorescent microspheres<sup>9</sup>.

In this setup, the absolute brightness of the fluorescent tags is a central design parameter, since it determines the achievable standoff distance for a given sensitivity of the device. However, the absolute brightness of highly fluorescent particles (e.g. fluorescent micro- and nanospheres<sup>10</sup>, quantum dots<sup>11</sup>, quantum dot virus nanoparticles<sup>12</sup>) has to the best of our knowledge not been determined, since knowledge of the relative brightness compared to molecular fluorophores is sufficient for most applications. Relative brightness is often expressed using the concept of Molecules of Equivalent Soluble Fluorophore (MESF)<sup>13-15</sup>.

Here, Nile-red fluorescent microspheres (Fluospheres, Invitrogen Inc.) are characterized with respect to their average absolute brightness and brightness variation, in a basic experimental setup. These measurements can be used as a guidepost in the design of devices relying on fluorescence detection, and anchor comparisons of relative brightness between fluorescent particles of different types.

### Methods

The brightness  $B$  of a fluorescent particle is defined here as:

$$B = \frac{P_{em}}{\Omega \times I_{ex}} \quad (1),$$

where  $I_{ex}$  is the excitation intensity, and  $P_{em}$  is the power of light emitted into the solid angle  $\Omega$ .

Since the absorptance and quantum yield of the fluorophore and the sensitivity of the detection setup are dependent on the spectral profile of excitation and emission light, the observed brightness is dependent on the details of the experiment. However, since the spectral dependence of these parameters is often known, the differences can be frequently estimated or neglected. For example, the achievable standoff distance scales with the fourth root of the particle brightness and is thus not very sensitive to small variations in brightness.

**Methods** (Fig. 1): Nile-red fluorescent microspheres with a 1  $\mu\text{m}$  diameter (product nr. F-8819, lot 91D2-1, Molecular Probes Inc.) were deposited and dried on microscopy cover slips (Fisherfinest<sup>TM</sup>, Premium Cover Glass, no 1, Fisher Scientific, Pittsburg, PA) and illuminated with the light from a Xenon arc lamp (Model LB-LS/30, Sutter Inc.). The excitation light was transmitted by a liquid light guide, collimated by a lens, and passed through an excitation filter (HQ535/35, bandpass center wavelength 535 nm, width 35 nm, 80% transmission, Chroma Inc.) to create uniform illumination of the sample with an intensity of 8 mW/cm<sup>2</sup> (measured with a hand-held power meter model #3803, New Focus Inc.). The sample fluorescence was passed through an emission filter (HQ595/50, centered at 595 nm with a width of 50 nm and 85% transmission, Chroma Inc.) and imaged by a lens (AR-coated achromat, focal length 60 mm, diameter 25 mm, Linos Inc.) placed at a distance of 185 mm from the sample onto a CCD camera (iXon DV887, ANDOR Inc., South Windsor, CT). The angle between the excitation and emission beams was 22.4°. It was confirmed that photobleaching was negligible.

The CCD camera sensitivity at the emission wavelength was calibrated by exposing it to collimated light from the Xenon arc lamp filtered by the emission filter (HQ595/50) and a neutral density filter (ND 3.0). Before

the insertion of the neutral density filter, the light intensity at the camera chip was  $22 \mu\text{W}/\text{cm}^2$ . After insertion of the neutral density filter, the camera registered 20,000  $\pm$  1,000 counts per pixel (background corrected, settings: temperature -50  $^{\circ}\text{C}$ , exposure time 100 ms, read-out rate 1 MHz@16 bit, pre-amplifier gain 4.1X, conventional amplifier selected, wells filled to 30% of capacity). With a pixel area of  $256 \mu\text{m}^2$ , this translates into a camera sensitivity of 0.29 aJ/count (or 0.9 photons/count).

Fluorescence microscopy images to characterize the distribution of microspheres in the sample were taken with an inverted epifluorescence microscope (TE2000U, Nikon Inc.) equipped with a 10x air objective and a 40x oil objective.

Fluorescence emission values were obtained from camera images by defining a rectangular region-of-interest (ROI) containing the fluorescent object, integrating the counts within the ROI, and subtracting the integrated counts of an adjacent section of the image of equal size but without fluorescent objects (background-ROI).

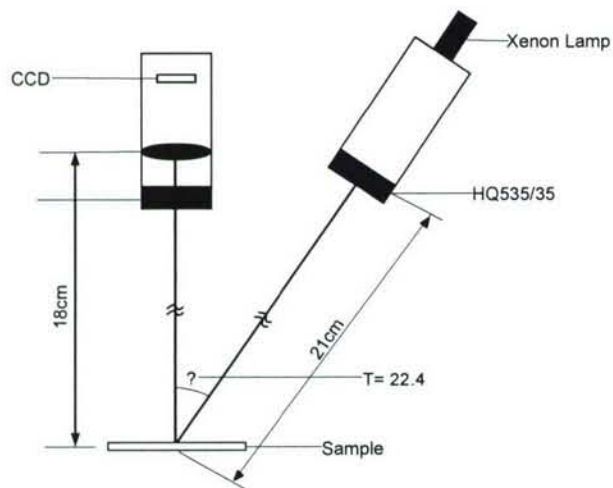


Figure 1: Schematic of the experimental setup.

**Results:** The relative brightness variation between individual microspheres was measured to be less than 13% (standard deviation of a set of 142 microspheres from 5 individual samples) by imaging the samples with a fluorescence microscope (10x objective). Quadratic fits to the brightness data as function of the location of the microspheres revealed that the systematic variation of brightness as function of position was less than 10% in x and y direction. Correcting for this systematic variation, which is presumably due to uneven illumination of the field of view did not significantly affect the standard deviation of the brightness.

Consequently, samples with 100-200 microspheres distributed over a 1 mm square were prepared. The distribution of microspheres was evaluated under the microscope using the 10x objective (Fig. 2a), the exact number of microspheres was counted using multiple images obtained with the 40x oil objective (Fig. 2c), and the fluorescence from the sample (Fig. 2b) was measured in the setup shown in Fig. 1. Four samples were measured, and the average number of counts per bead was determined to be  $265 \pm 27$  (average  $\pm$  stdev).

The brightness  $B$  of a microsphere can now be calculated from equation 1, according to:

$$B = \frac{C_{em} \times S_{camera} \times T_{F,L}}{t_{exposure} \times I_{ex}} \bigg/ \frac{\pi D_L^2}{4L_{S-C}} \quad (2),$$

Where  $C_{em} = 260$  – detected counts per microsphere,  $S_{camera} = 0.17 \text{ aJ}/\text{count}$  – camera sensitivity,  $T_{F,L} = 0.8$  – transmission of emission filter and collection lens,  $t_{exposure} = 100 \text{ ms}$  – exposure time,  $I_{ex} = 8 \text{ mW}$  – excitation intensity,  $D_L = 25 \text{ mm}$  – diameter of collection lens, and  $L_{S-C} = 185 \text{ mm}$  – distance between sample and collection lens.

The result of this calculation is an average brightness per Nile-red fluorescent microspheres with a  $1 \mu\text{m}$  diameter (product nr. F-8819, lot 91D2-1, Molecular Probes Inc.) of  $3 \pm 1 \times 10^{-16} \text{ m}^2/\text{sr}$ . The principal sources of error are  $C_{em}$ ,  $S_{camera}$  (due to the uncertainty in the neutral density filter absorption), and  $T_{F,L}$ .

The above result does not take into account the complex angular dependence of the fluorescence intensity on polarization, emission angle and particle size and form factor<sup>16</sup>. In the present case both excitation and emitted light are unpolarized, the fluorophores are randomly oriented and distributed within spherical particles. At the chosen angle of 22.4° between excitation and detection axis, theoretical and experimental results for fluorescent spheres of similar size<sup>17</sup> indicate that the fluorescence is less than 5% reduced compared to an angle of 0°. Given the significantly larger experimental error of our measurement, we decided not to correct for this.

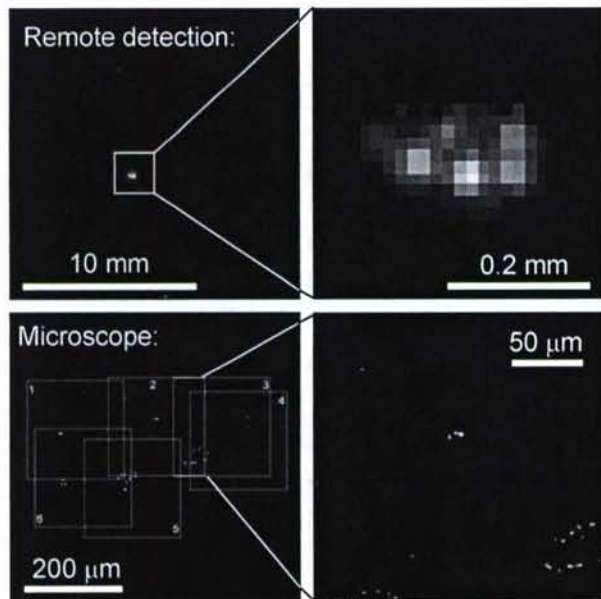


Figure 2: A sample of microspheres imaged by (a) the fluorescence microscope with 10x objective, (b) the setup shown in Fig. 1, and (c) the microscope with 40x objective.

**Discussion and Conclusion:** The utility of the determined absolute brightness can be illustrated by the following example calculation: A typical LIDAR system<sup>9, 18-21</sup> can deliver a pulse energy of 0.3 J at a wavelength of 532 nm into a 0.2 m spot at a distance of 500 m and collect fluorescence with a 20 cm telescope. Using our CCD camera with a read-out noise of 20 counts and a sensitivity of 0.2 aJ/count and collection optics with 80% transmission, a signal-to-noise ratio (SNR) of one is reached for an object with a brightness of  $8 \times 10^{15} \text{ m}^2/\text{sr}$ . Thus, an acceptable SNR of five would require on the order of 100 fluorescent microspheres to be illuminated simultaneously by the pulse. This number is increased by the unavoidable background fluorescence and losses due to encapsulation of the fluorescent particles in the envisioned “smart dust” device, but can be reduced by averaging over multiple pulses. Conversely, given a certain number of fluorescent microspheres, a maximal stand-off distance can be estimated.

1. M. J. Sailor and J. R. Link, *Chemical Communications*, 2005, 1375-1383.
2. T. Frische, *Ecotoxicology and Environmental Safety*, 2002, **51**, 133-144.
3. H. Hess and V. Vogel, *Reviews in Molecular Biotechnology*, 2001, **82**, 67-85.
4. H. Hess, G. D. Bachand and V. Vogel, *Chemistry - A European Journal*, 2004, **10**, 2110-2116.
5. George D. Bachand, Susan B. Rivera, A. Carroll-Portillo, H. Hess and M. Bachand, *Small*, 2006, **2**, 381-385.
6. S. Ramachandran, K.-H. Ernst, George D. Bachand, V. Vogel and H. Hess, *Small*, 2006, **2**, 330-334.
7. R. Seetharam, Y. Wada, S. Ramachandran, H. Hess and P. Satir, *Lab on a Chip*, 2006, **6**, 1239-1242.
8. B. D. Martin, C. M. Soto, A. S. Blum, K. E. Sapsford, J. L. Whitley, J. E. Johnson, A. Chatterji and B. R. Ratna, *Journal of Nanoscience and Nanotechnology*, 2006, **6**, 2451-2460.
9. R. J. Simonson, P. J. Hargis, M. S. Johnson, R. L. Schmitt and B. G. Hance, *Proceedings of the SPIE - The International Society for Optical Engineering* 2001, **4394**, 879-889.
10. R. P. Haugland, *Handbook of Fluorescent Probes and Research Chemicals*, Molecular Probes, Eugene, 2004.
11. W. C. W. Chan and S. M. Nie, *Science*, 1998, **281**, 2016-2018.

12. Amy S. Blum, Carissa M. Soto, Charmaine D. Wilson, Tina L. Brower, Steven K. Pollack, Terence L. Schull, A. Chatterji, T. Lin, John E. Johnson, C. Amsinck, P. Franzon, R. Shashidhar and Banahalli R. Ratna, *Small*, 2005, **1**, 702-706.
13. A. Schwartz, L. Wang, E. Early, A. Gaigalas, Y. Z. Zhang, G. E. Marti and R. F. Vogt, *Journal of Research of the National Institute of Standards and Technology*, 2002, **107**, 83-91.
14. A. K. Gaigalas, L. L. Wang, A. Schwartz, G. E. Marti and R. F. Vogt, *Journal of Research of the National Institute of Standards and Technology*, 2005, **110**, 101-114.
15. A. Schwartz, A. K. Gaigalas, L. L. Wang, G. E. Marti, R. F. Vogt and E. Fernandez-Repollet, *Cytometry Part B-Clinical Cytometry*, 2004, **57B**, 1-6.
16. S. C. Hill, R. G. Pinnick, S. Niles, N. F. Fell, Y. L. Pan, J. Bottiger, B. V. Bronk, S. Holler and R. K. Chang, *Applied Optics*, 2002, **41**, 4432-4432.
17. S. D. Druger and P. J. McNulty, *Applied Optics*, 1983, **22**, 75-82.
18. P. Weibring, H. Edner and S. Svanberg, *Applied Optics*, 2003, **42**, 3583-3594.
19. J. R. Simard, G. Roy, P. Mathieu, V. Laroche, J. McFee and J. Ho, *Ieee Transactions on Geoscience and Remote Sensing*, 2004, **42**, 865-874.
20. K. J. Lee, Y. Park, A. Bunkin, R. Nunes, S. Pershin and K. Voliak, *Applied Optics*, 2002, **41**, 401-406.
21. P. Hargis, A. Lang, R. Schmitt, T. Henson, J. Daniels, D. Jordan, K. Sch Schroder and I. Shokair, in *4th Joint Workshop on Standoff Detection for Chemical and Biological Defense*, Williamsburg, VA, 1998.

### (C) Velocity optimization for pick-up of optical tags by molecular shuttles

**Abstract:** Molecular shuttles, active nanoscale transport systems based on biomolecular motors and their associated filaments, have been developed to serve as conveyor belts in future molecular factories, which assemble complex nanoscale structures in a controlled sequence of steps. Here we show that the molecular shuttle velocity has to be optimized to facilitate attachment of nanospheres via biotin-streptavidin linkages as a result of the complex binding energy landscape of the linkages. In essence, biotin and streptavidin act as glue which has to harden before stress can be applied.

The attachment of nanoscale cargo to motor protein-powered molecular shuttles is a key functional element of the overall design.<sup>1,2</sup> Several investigations have explored the influence of cargo type, size and density<sup>3-9</sup> as well as of different linkages, including biotin - streptavidin, cyclodextrin host - guest<sup>10</sup>, malachite green - aptamer<sup>11</sup>, DNA - DNA<sup>12</sup>, and antibody - antigen<sup>13-15</sup>. Using functionalized microtubules gliding on kinesin motor protein-coated surfaces as shuttle design, we investigate for the first time the effect of shuttle velocity on cargo attachment via biotin - streptavidin linkages and discover an unexpected optimum in the shuttle velocity.

In the experiments (Fig. 1), kinesin motor proteins are adsorbed to a surface precoated with casein, biotinylated microtubules adhere to the kinesin and are subsequently coated with rhodamine-labeled streptavidin. The microtubule gliding velocity was controlled via the concentration of the kinesin substrate ATP and varied between 50 nm/s and 450 nm/s. Finally, biotinylated fluorescein-labeled nanospheres were added in concentrations ranging from 25 pM to 100 pM, which resulted in surface densities of 250 to 1400 nanospheres within a field of view of the fluorescence microscope (80  $\mu\text{m}$  x 80  $\mu\text{m}$ ). Nanospheres attached to microtubules only as a result of collisions between gliding microtubules and nanospheres attached to the surface. Binding of nanospheres from solution to moving microtubules was never observed, and stationary microtubules (in the absence of ATP) did not capture nanospheres from solution.

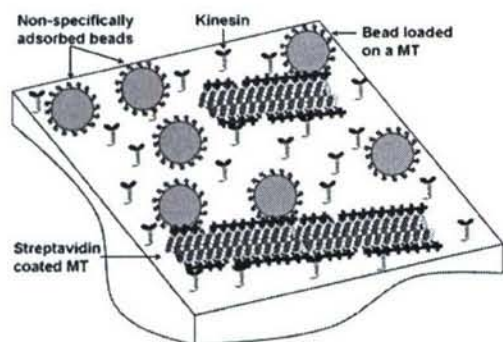


**Figure 1:** Sketch of principle. Biotinylated MTs are coated with rhodamine-labeled streptavidin. Biotinylated polystyrene fluorescein nanospheres (40nm diameter) adhering to the surface are picked up by the streptavidin coated MTs as they move upon the kinesin coated surface.

The attachment and subsequent transport of nanospheres by microtubules is readily apparent not only when rhodamine-labeled microtubules are imaged due to the residual fluorescence of fluorescein-labeled nanospheres (Fig. 2), but also when only nanospheres are imaged due to the movement of distinct groups of nanospheres. Control experiments were carried out in which 10% rhodamine- and 90% biotin-labeled MTs were used but the streptavidin coating step was omitted. These microtubules do not capture any nanospheres from the surface which proves that the capture of nanospheres occurred specifically through the streptavidin-biotin chemistry. A striking dependence of nanosphere attachment on microtubule velocity can be illustrated by overlays of images from the rhodamine and fluorescein channel (Fig. 3).

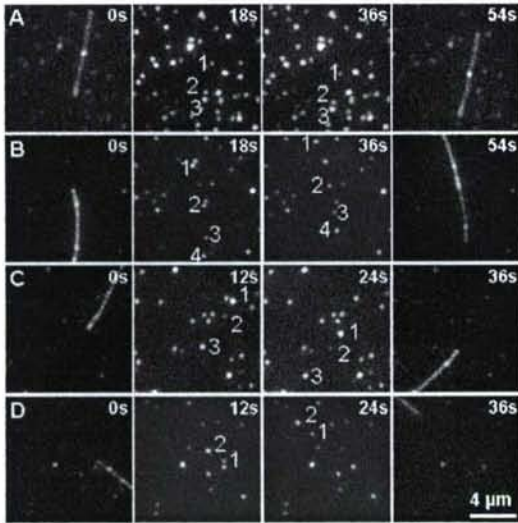


**Figure 2:** Time lapse images of attachment experiments at different ATP concentrations. Microtubules covered with rhodamine-labeled streptavidin are imaged in the first and last image of a row, and fluorescein-labeled biotinylated nanospheres are imaged in the center. Microtubules are moving with a velocity of 50nm/s in row A, 175nm/s in row B, 325nm/s in row C and 450nm/s in row D.

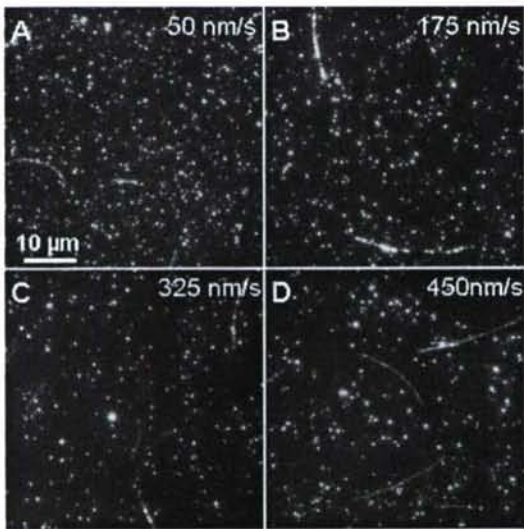


**Figure 3:** Loading of microtubules (false-colored red) moving at 50nm/s (in A), 175nm/s (in B), 325nm/s (in C) and 450nm/s (in D) 10 minutes after the injection of nanospheres (false-colored green). It can be clearly seen that loading in (B) is the maximum and in (D) is the minimum.

Since the attachment occurs only via surface collisions, the attachment rate can be expressed by:

$$k_{\text{attachment}} = S_{\text{MT}}(v)k_{\text{collision}} = S_{\text{MT}}(v)\sigma_{\text{spheres}}d_{\text{MT}}v$$

The velocity-dependent sticking probability  $S_{\text{MT}}(v)$  was determined by measuring nanosphere surface density  $\sigma_{\text{spheres}}$  and gliding velocity  $v$ , estimating the grasp  $d_{\text{MT}}$  of the microtubule as 150 nm based on the geometry of kinesin-bound microtubule<sup>16</sup> and nanosphere, and calculating the attachment rate  $k_{\text{attachment}}$  by dividing the total number of attached nanospheres by the total number of moving microtubules in the field of view at 10 minutes after nanosphere injection (Fig. 4).  $S_{\text{MT}}(v)$  is almost unity for speeds less than 200nm/s but decreases dramatically at higher velocities.

The sticking probability for each microtubule  $S_{\text{MT}}$  is a result of the repeated attempts of streptavidins attached to the microtubule to grasp the biotinylated microsphere. By measuring the biotinylation ratio of the tubulin ( $0.6 \pm 0.1$  biotins per tubulin) and the average length of the microtubules ( $4.5 \pm 0.4 \mu\text{m}$ ) we determined that  $n=340 \pm 90$  attempts to form a linkage were made during each collision between a microtubule and a nanosphere.  $S_{\text{MT}}$  is thus given by  $S_{\text{MT}} = 1 - (1 - S_1)^{340}$  where  $S_1$  is the likelihood that a linkage is successfully formed during an individual biotin-streptavidin encounter.

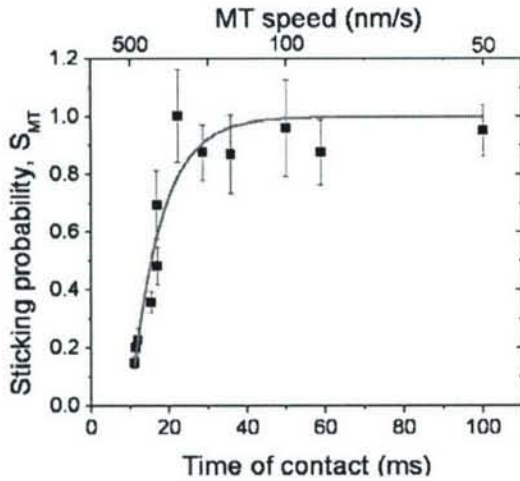


**Figure 4:** Experimentally observed  $S_{MT}$  versus time of interaction of each bond. It is fitted with the probability function for filling up the equilibrium binding state of the biotin-streptavidin bond after taking into consideration the multiple interactions which take place between the streptavidin along the length of the MT and biotin on the nanosphere in every MT-bead collision.

We propose that the velocity dependence of  $S_1$  can be understood by considering the velocity-dependent time of contact  $t_c$ . Assuming the size of the streptavidin molecule to be 5 nm,<sup>17,18</sup> the time of contact decreases from 100 ms for a microtubule moving at 50 nm/s to 10 ms for a microtubule moving at 500 nm/s (Fig. 4).

Pincet et al.<sup>19</sup> found that biotin-streptavidin linkages which were allowed to form over long periods of time were stronger than the linkages which were subjected to pulling forces immediately after formation. This has been explained to result from the shape of the biotin-streptavidin energy landscape, which displays two metastable states in addition to the energy minimum (Fig. 5)<sup>20</sup>. During the initial contact between biotin and streptavidin, the outermost state is populated. In the absence of an opposing force, the second metastable state is populated on a microsecond timescale, followed by a transition to the equilibrium state within seconds. In the presence of an opposing force, which is here provided by the attachment of the nanosphere to the surface, the energy landscape is altered, and the kinetics of the formation of a stable linkage changes.

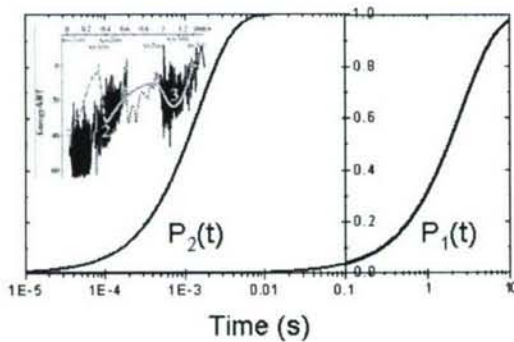


**Figure 5:** Filling up of energy landscape minima as a function of time. Inset shows the energy landscape of a biotin-streptavidin bond as obtained by Pincet et.al. Apart from the most stable equilibrium binding state 1, there are two metastable states (2 and 3). Plotted are the probabilities of a bond that is initially in the outermost minimum to be present in states 2 and 1, assuming a force of 24 pN opposed to bond formation.

The dependence of  $S_1$  on the time of contact  $t_c$  can be calculated for a given opposing force using the parameters provided by Pincet et al.<sup>19</sup>. A resistive force of 24 pN (+13/-17 pN) provides the best fit to the experimental data of the dependence of  $S_1$  on  $t_c$  (Fig. 4).

In summary, the attachment rate to a microtubule is given by:

$$k_{attachment} = \sigma_{spheres} \cdot d_{MT} \cdot v [1 - (\exp(-.38 * (5/v - .01)))^n]$$

The attachment rate rises linearly from zero with increasing velocity, reaches a maximum at a velocity of about 250 nm/s, and drops again to zero at a velocity of 500 nm/s (Fig. 6). The optimum velocity is independent of bead density or microtubule grasp but depends on the attachment strength of the nanospheres. It is striking that the attachment rate at typical microtubule gliding velocities of 0.5  $\mu\text{m/s}$  is near zero.

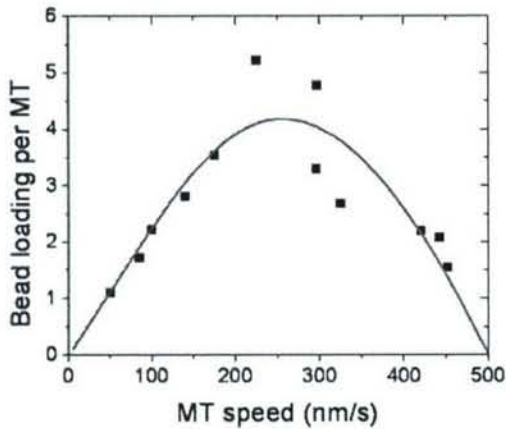


**Figure 6:** Microtubule attachment rate as a function of speed for a nanosphere surface density of  $0.25\mu\text{m}^{-2}$  (red curve). The black data points are the actually observed values which have been normalized for a bead density of  $0.25\mu\text{m}^{-2}$ .

In summary, the existence of an optimal velocity cargo attachment to molecular shuttles is a consequence of the complex binding energy landscape of the biotin-streptavidin linkages. The behavior of biotin-streptavidin linkages is best captured by the “glue” metaphor, which emphasizes that a certain curing time is required to achieve the ultimate strength of the linkage. In contrast, lectin-selectin or mannose-FimH catchbonds function as “hooks” which gain strength under load, DNA-DNA linkages act like “adhesive tape”, and Nickel-His-tag linkages resemble “magnets”. Translating the description of molecular building blocks and their behavior into appropriate metaphors is important for the design and understanding of nanosystems, since it enables the correct application of our engineering intuition honed by decades of experience with macrosystems.

#### Materials and methods:

The experiments were performed in a  $100\mu\text{m}$  high and  $1\text{cm}$  wide flow cells assembled from two coverslips and double stick-tape<sup>21</sup>. First, a solution of casein ( $0.5\text{mg/mL}$ , Sigma) dissolved in BRB80 ( $80\text{mM}$  PIPES,  $1\text{mM}$   $\text{MgCl}_2$ ,  $1\text{mM}$  EGTA, pH 6.9) was injected into the flow cell, since casein adsorbed to surfaces reduces the denaturation of kinesin. After 5 min, a kinesin solution was injected and after 5 min exchanged against a motility solution containing  $0.8\mu\text{g/mL}$  biotinylated microtubules (MTs), ATP ( $20\mu\text{M}$ ,  $50\mu\text{M}$ ,  $100\mu\text{M}$  or  $1\text{mM}$ ) and an antifade system ( $20\text{mM}$  D-glucose,  $20\mu\text{g/mL}^{-1}$  glucose oxidase,  $8\mu\text{g/mL}$  catalase,  $10\text{mM}$  dithiothreitol). Five minutes were allowed for MT attachment after which  $20\text{nM}$  Alexa568-labeled streptavidin (Molecular Probes) in motility solution without MTs was perfused into the flow cell and incubated for five minutes to cover all the biotin sites on the MTs<sup>14</sup>. Finally, after three washes with motility solution without MTs, biotin-labeled  $40\text{nm}$  nanospheres loaded with fluorescein dye (Molecular Probes) at different concentrations ( $25\text{-}100\text{pM}$ ) in motility solution without MTs were introduced into the flow cell. The flow cell was mounted on the microscope stage and the time elapsed since bead introduction was recorded. An Eclipse TE2000-U fluorescence microscope (Nikon, Melville, NY) equipped with a  $100\times$  oil objective (N.A. 1.45), an X-cite 120 lamp (EXFO, Ontario, Canada), a FITC filter cube (#48001), a TRITC filter cube (#48002, Chroma Technologies, Rockingham, VT) and an iXon EMCCD camera (ANDOR, South Windsor, CT) was used to image MTs and nanospheres on the bottom surface of flow cells. Exposure time was kept fixed at  $0.5\text{s}$  although the time between exposures was varied from 4 to 8 seconds depending on MT speeds. Uninhibited transport of nanosphere-loaded MTs at nanosphere concentrations as high as  $1\text{nM}$  was observed if the excitation light intensity was reduced thirty-fold, indicating that the previously described limit of  $10\text{pM}$  is a result of photodamage.

*Kinesin and microtubules.* A kinesin construct consisting of the wild-type, full-length *Drosophila melanogaster* kinesin heavy chain and a C-terminal His-tag was expressed in *Escherichia coli* and purified using a Ni-NTA column<sup>22</sup>. MTs were prepared by polymerizing  $20\mu\text{g}$  of biotin labeled-tubulin (Cytoskeleton Inc., Denver CO) in  $6.5\mu\text{L}$  of growth solution containing  $4\text{mM}$   $\text{MgCl}_2$ ,  $1\text{mM}$  GTP and 5% DMSO (v/v) in BRB80 buffer for 30 min at  $37^\circ\text{C}$ . The MTs with lengths between  $1$  and  $20\mu\text{m}$  were 100-fold diluted and stabilized in  $10\mu\text{M}$  Paclitaxel (Sigma, Saint Louis MO). A biotin quantitation kit (Invitrogen Inc.) was used to estimate that there are  $0.6\pm 0.1$  moles of biotin per mole of tubulin.

## References:

- 1 Hess, Henry & Vogel, Viola Molecular shuttles based on motor proteins: Active transport in synthetic environments. *Reviews in Molecular Biotechnology* 82 (1), 67-85 (2001).
- 2 van den Heuvel, M. G. L. & Dekker, C. Motor proteins at work for nanotechnology. *Science* 317 (5836), 333-336 (2007).
- 3 Hess, Henry *et al.* Light-Controlled Molecular Shuttles Made from Motor Proteins Carrying Cargo on Engineered Surfaces. *Nano Letters* 1 (5), 235-239 (2001).
- 4 Diez, Stefan *et al.* Stretching and Transporting DNA Molecules Using Motor Proteins. *Nano Letters* 3 (9), 1251-1254 (2003).
- 5 Bachand, G. D. *et al.* Assembly and transport of nanocrystal CdSe quantum dot nanocomposites using microtubules and kinesin motor proteins. *Nano Letters* 4 (5), 817-821 (2004).
- 6 Patolsky, F., Weizmann, Y., & Willner, I. Actin-based metallic nanowires as bio-nanotransporters. *Nature Materials* 3 (10), 692-695 (2004).
- 7 Mansson, A. *et al.* In vitro sliding of actin filaments labelled with single quantum dots. *Biochemical and Biophysical Research Communications* 314 (2), 529-534 (2004).
- 8 Bachand, M., Trent, A. M., Bunker, B. C., & Bachand, G. D. Physical factors affecting kinesin-based transport of synthetic nanoparticle cargo. *Journal of Nanoscience and Nanotechnology* 5 (5), 718-722 (2005).
- 9 Boal, A. K., Bachand, G. D., Rivera, S. B., & Bunker, B. C. Interactions between cargo-carrying biomolecular shuttles. *Nanotechnology* 17 (2), 349-354 (2006).
- 10 Kato, K. A., Goto, R., Kato, K., & Shibakami, M. Microtubule-cyclodextrin conjugate: Functionalization of motile filament with molecular inclusion ability. *Bioscience Biotechnology and Biochemistry* 69 (3), 646-648 (2005).
- 11 Hirabayashi, M. *et al.* Malachite green-conjugated microtubules as mobile bioprobes selective for malachite green aptamers with capturing/releasing ability. *Biotechnology and Bioengineering* 94 (3), 473-480 (2006).
- 12 Taira, S. *et al.* Selective detection and transport of fully matched DNA by DNA-loaded microtubule and kinesin motor protein. *Biotechnology and Bioengineering* 95 (3), 533-538 (2006).
- 13 Bachand, George D. *et al.* Active Capture and Transport of Virus Particles Using a Biomolecular Motor-Driven, Nanoscale Antibody Sandwich Assay. *Small* 2 (3), 381-385 (2006).
- 14 Ramachandran, Sujatha *et al.* Selective Loading of Kinesin-Powered Molecular Shuttles with Protein Cargo and its Application to Biosensing. *Small* 2 (3), 330-334 (2006).
- 15 Brunner, Christian, Wahnes, Christian, & Vogel, Viola Cargo pick-up from engineered loading stations by kinesin driven molecular shuttles. *Lab on a Chip* 7 (10), 1263-1271 (2007).
- 16 Kerssemakers, Jacob, Howard, Jonathon, Hess, Henry, & Diez, Stefan The distance that kinesin holds its cargo from the microtubule surface measured by fluorescence-interference-contrast microscopy. *PNAS* 103 (43), 15812-15817 (2006).
- 17 Huang, N. P. *et al.* Biotin-Derivatized Poly(L-lysine)-g-poly(ethylene glycol): A Novel Polymeric Interface for Bioaffinity Sensing. *Langmuir* 18 (1), 220-230 (2002).
- 18 Frey, Wolfgang *et al.* Electron Crystallographic Analysis of Two-Dimensional Streptavidin Crystals Coordinated to Metal-Chelated Lipid Monolayers. *Biophys. J.* 74 (5), 2674-2679 (1998).
- 19 Pincet, F. & Husson, J. The solution to the streptavidin-biotin paradox: The influence of history on the strength of single molecular bonds. *Biophysical Journal* 89 (6), 4374-4381 (2005).
- 20 Pierres, Anne, Touchard, Dominique, Benoliel, Anne-Marie, & Bongrand, Pierre Dissecting Streptavidin-Biotin Interaction with a Laminar Flow Chamber. *Biophys. J.* 82 (6), 3214-3223 (2002).
- 21 Howard, J., Hunt, A. J., & Baek, S. Assay of microtubule movement driven by single kinesin molecules. *Methods Cell Biol* 39, 137-147 (1993).
- 22 Coy, D. L., Wagenbach, M., & Howard, J. Kinesin takes one 8-nm step for each ATP that it hydrolyzes. *J Biol Chem* 274 (6), 3667-3671 (1999).

## (D) Proof-of-principle demonstration of basic biomolecular motor-powered sensor

**Abstract:** The objective of the subproject was to provide a proof-of-principle demonstration of analyte capture, tagging and deposition within the most basic physical structure and the most easily captured analyte. To this end, a circular well structure was designed and fabricated using SU8 photoresist. Controlled deposition of biotinylated microtubules and biotinylated fluorescent microspheres in the center of the circular well created a deposition zone at the perimeter of the well, which was initially free of fluorescent microspheres. Injection of the streptavidin analyte and subsequent photolytic release of caged ATP led to capture of streptavidin by microtubules, pick-up of microspheres, and finally immobilization of microsphere-carrying microtubules at the wall of the well. This proves that molecular shuttles can drive the analyte-dependent transport of fluorescent tags and provides the basis for optimization at the systems level.

**Introduction:** During the course of the Biomolecular Motors Program it became apparent that individual technological hurdles (e.g. storage, brighter optical tags, optimal velocity) can be solved, and that the remaining central challenge in the drive towards a functioning device was the integration of all components. In the spirit of the DARPA Biomolecular Motor program, which attacks the key problems first, the Hess group began to expend a substantial portion of the effort on the fabrication of a prototype.

The initial approach aimed at the fabrication of an enclosed, multi-chamber Polyurethane structure with distinct access ports (Fig. 1). However, testing of the design revealed a series of problems:

- (1) Evaporation at injection ports lead to rapid, unintended fluid flow within the device.
- (2) Gliding microtubules often got stuck on defective motors, which reveals problems with motor protein density and activity within the chambers.
- (3) Parallel manufacturing of the device is impossible.

As a result, the initial approach was abandoned in favor of a more sophisticated fabrication strategy, which replaces replica molding with photolithography and takes advantage of materials (glass, SU8 photoresist) previously utilized in kinesin-based devices<sup>1,2</sup>.

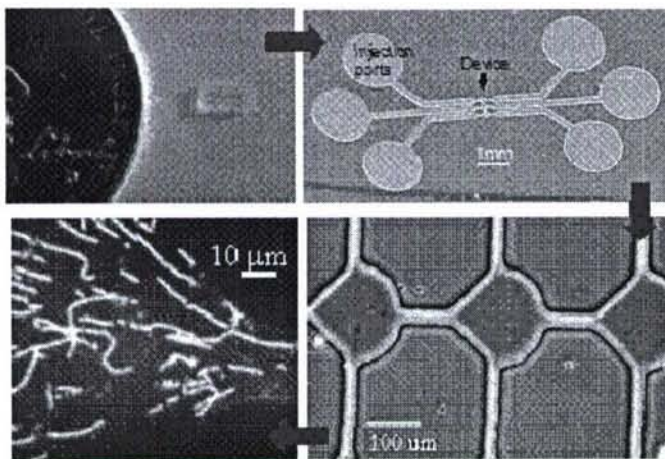


Fig. 1: A three chamber polymeric device with injection ports as the initial design of the smart dust sensor housing.

Initial tests of multi-chamber designs fabricated with glass substrates and SU8 sidewalls revealed an unexpected phenomenon: Microtubules were immobilized upon contact with the sidewall, rather than being redirected and guided along the sidewall. This phenomenon is likely a result of our processing conditions leading to a rough and possibly slightly delaminating sidewall, which provides the ideal conditions to immobilize microtubules on contact.

This phenomenon however, generates the possibility for a dramatic simplification of the device design (Fig. 2). Since the wall provides a distinct deposition zone, a circular device replacing multiple chambers with a single chamber containing functional, radially separated zones becomes possible. This design is further facilitated by the fabrication of an overhang<sup>3</sup> at the photoresist wall, which reduces the deposition of optical tags near the wall and thus enables the separation of nanospheres transported by the microtubules and nanospheres settling to the surface after their injection during the assembly process.

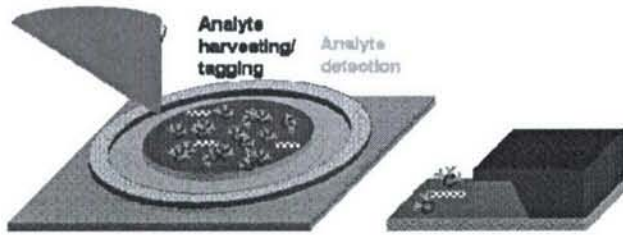


Figure 2: Sketch of circular, single-chamber device. The overhanging side wall prevents optical tags from settling near the wall during assembly. Analyte-dependent transport of optical tags by microtubules to the wall is followed by immobilization of tags and microtubules at the wall.

In the following, the fabrication and testing of the single-chamber device will be described.

**Methods:** *Manufacturing of photo mask:* The layout of the photo mask was drawn using progeCAD LT 2006 (progeSOFT, Como, Italy) and transferred to a precision laser photoplot (resolution 1/40.64 mil, Photoplot Store, Colorado Springs, CO).

*Photolithography of SU8:* The substrate, round cover slips ( $\varnothing$  25 mm, No. 2, Fisher brand, Fisher Scientific, Hampton, NH), was pretreated by rinsing with acetone, methanol and water. To dehydrate the surface the substrate was baked for 10 min at 200 °C on a contact hot plate. Approximately 1 mL of SU8-2015 (MicroChem, Newton, MA) was spin coated (Headway Research, Garland, TX) onto the substrate (static dispense; spread cycle: ramp to 500 rpm at 100 rpm/s acceleration; spin cycle: ramp to 2000 rpm at 300 rpm/s acceleration and hold for 30 s). Edge bead was mechanically removed with a cotton tipped applicator. The resist was soft baked for 1 min at 65 °C and for 3 min at 95 °C, exposed for 25 s in a MJB3 mask aligner (i-Line, 6 mW/cm<sup>2</sup>) (Suss MicroTec, Garching, Germany) and post baked for 1 min at 65 °C and for 2 min at 95 °C on a contact hot plate. The structures were developed for 10 min in a Branson 200 ultrasonic bath (Branson, Danbury, CT) using SU8 developer (MicroChem, Newton, MA). Following development, the substrate was rinsed briefly with isopropyl alcohol and then dried with a gentle stream of nitrogen. The thickness of the resist was measured using a Dektak II (Sloan now Veeco, Woodbury, NY).

*Kinesin and microtubule preparation:* A kinesin construct consisting of the wild-type, full-length *Drosophila melanogaster* kinesin heavy chain and a C-terminal His-tag was expressed in *Escherichia coli* and purified using a Ni-NTA column.<sup>4</sup> Microtubules were prepared by polymerizing 20  $\mu$ g of rhodamine-labeled and biotinylated tubulin (both Cytoskeleton, Denver, CO) respectively in 6.5  $\mu$ L of growth solution containing 4 mM MgCl<sub>2</sub>, 1 mM GTP and 5% DMSO (v/v) in BRB80 buffer (80 mM PIPES, 1 mM EGTA, 2 mM MgCl<sub>2</sub>, pH 6.9) for 30 min at 37 °C.<sup>5</sup> The microtubules were subsequently diluted 100-fold into BRB80 containing 10  $\mu$ M paclitaxel.

*Assembly of the smart dust sensor:* The whole assembly and operation of the smart dust sensor was carried out under minimal light intensity to prevent accidental release of caged ATP. Further to prevent dry-up, degradation and photobleaching the sensor was kept under an atmosphere of humidified nitrogen except for solution exchange. Humidification was obtained by bubbling nitrogen gas through two scrubber flasks filled water. The sensor surface was cleaned by rinsing with ethanol and water. Solution exchange on the sensor surface was carried out by microliter fluid handling techniques using two 100  $\mu$ L piston-driven air displacement pipettes. The solution were applied as a droplet onto the sensor surface and exchanged by suction and subsequent deposition of a new droplet. The surfaces of the sensor was wetted with BRB80 (5 min, 100  $\mu$ L), coated with casein (0.5 mg/ml in BRB80 for 5 min, 100  $\mu$ L) and kinesin (~10 nM in BRB80 with 0.5 mg/ml casein and 0.1 mM caged ATP for 10 min, 100  $\mu$ L). The surface was then "washed" once with antifade solution (0.2 mg/mL casein, 0.1 mM caged ATP, 20 mM D-glucose, 20  $\mu$ g/mL glucose oxidase, 8  $\mu$ g/mL catalase and 1 % DTT (v/v) in BRB80, 100  $\mu$ L). A motility solution containing biotinylated and rhodamine-labeled microtubules (ratio 10:1) (15.4  $\mu$ g/mL biotinylated MTs, 1.6  $\mu$ g/mL rhodamine-labeled MTs, 0.1 mg/mL casein, 0.1 mM caged ATP, 20 mM D-glucose, 20  $\mu$ g/mL glucose oxidase, 8  $\mu$ g/mL catalase and 1 % DTT (v/v) in BRB80 for 5 min, 100  $\mu$ L). The surface was then "washed" with antifade solution (100  $\mu$ L) and incubated with a suspension containing biotinylated fluorescein microspheres ( $\varnothing$  40 nm, FluoSpheres F8766, Molecular Probes, Eugene, OR) (5 min, 100  $\mu$ L). This bead suspension was made prior by suspending 1  $\mu$ L of the microsphere stock suspension in 49  $\mu$ L BlockAid Blocking Solution (Molecular Probes, Eugene, OR) and sonicating this suspension for 5 min in an ultrasonic bath. This suspension was then diluted 20 times in antifade solution to

give the final concentration (0.5 nM FluoSpheres in antifade solution). After “washing” the surface thrice with antifade solution (3x 100  $\mu$ L) the sensor was ready for operation.

*Operation of the smart dust sensor:* To load analyte into the sensor the antifade solution was exchanged against a solution of alexa-fluor 568 labeled streptavidin (Molecular Probes, Eugene, OR) (1.0 nM streptavidin in antifade solution, 100  $\mu$ L). Caged ATP was subsequently released by illuminating the sensor for 90 s with UV light. For this purpose a LB-LS/30 light source (Sutter Instrument Company, Novato, CA) equipped with a UV band path filter (D350/50x, Chroma Technologies, Rockingham, VT) was used. The intensity at the sample was measured using a UV light meter (UV-340, Mannix, New York, NY) to be 1.40 mW/cm<sup>2</sup>.

*Read-out of the smart dust sensor:* An Eclipse TE2000-U fluorescence microscope (Nikon, Melville, NY) with a 100x oil objective (N.A. 1.4) and a 10x air objective (N.A. 0.3), a X-cite 120 light source (EXFO, Ontario, Canada), a rhodamine (#48002, Ex 535 nm, Em 610 nm) and a fluorescein filter cube, (#48001, Ex 480 nm, Em 535 nm, both cubes Chroma Technologies, Rockingham, VT) and an iXon EMCCD camera (ANDOR, South Windsor, CT) were used to image microtubules on the surface of the sensor cells.

## Results:

*Manufacturing of photo mask:* Since the basic layout of the smart dust sensor consists out of a simple circular pattern with no high-resolution features, laser photoplots on a flexible polymer film were chosen for photolithography. Compared to conventional chrome on glass contact masks photoplots are low cost and readily available within 2 days and therefore allow a rapid prototyping of photoresist patterns. The photoplotter used is capable of printing with a resolution up to 1/40.64 mil. This corresponds to minimum sizes of 0.25 mil (6  $\mu$ m) for linear features and 0.4 mil (10  $\mu$ m) for round/square features and therefore easily exceeds the needed minimum feature size of the smart dust sensor. The layout of the photomask was designed to fit multiple smart dust sensors of different sizes, ranging from 150  $\mu$ m to 750  $\mu$ m in diameter, onto a single substrate.

*Photolithography of SU8:* In order for the sensor to provide the needed volume for the incorporation of fluids the photoresist layer has to be thicker than the thickness of conventional photolithography resists, which typically form layers of 1-2  $\mu$ m. To create deep well like structures with 20  $\mu$ m deep walls the photoresist SU8-2015 was chosen. Besides being available as a thick photoresist, SU8 also shows low autofluorescence which is important for achieving a high signal-to-noise ration during the fluorescence read-out of the sensor. In addition microtubule motility was shown in the past to be impaired on SU8 surfaces; therefore the motility can be largely restricted to the substrate surface.<sup>1</sup> Round glass cover slips were chosen as the substrate, since glass is known to provide the most stable microtubule motility. Due to a large difference in the thermal expansion coefficients of glass (~10 ppm/K) and SU8 (50 ppm/K) photolithography of SU8 on glass can lead to highly stressed films which tend to delaminate or crack. To counteract delaminating, care was taken to assure a good adhesion by solvent rinsing and dehydrating the glass substrates. In addition to prevent thermal stress cracking, a two temperatures soft and post exposure bake were used. Differing from thin resists, sharp features were not attainable during development by simple agitation of the substrate in the developer. To assure complete removal of undeveloped resist the development was carried out in an ultrasonic bath.

The thickness of the resist and therefore the deepness of the wells were measured to be  $18 \pm 1$   $\mu$ m, which is in good conformity with the expected thickness of 20  $\mu$ m according to the product manual. During further inspection of the photoresist sidewalls, a pronounced T-top and a strong negative sidewall slope were observed. This T-topping is caused by overexposure of the photoresist top layer. The mercury vapor light source in the MJB3 mask aligner produces besides the exposure light at 365 nm (i-line) also light at 313 nm and 334 nm. This short wavelength UV light is strongly absorbed by the top layer of SU8 and causes formation of acids, which diffuse outward and concentrate at the top edge. These acids lead during the post exposure bake to a strong cross-linking of the SU8 in this area and therefore a responsible for the T-topping. [Rumpf, micro-photonic systems utilizing SU-8] Though formation of a T-top can be minimized by using an appropriate UV filter, e.g. Hoya UV-34, T-top and negative side wall slope proved to be useful in the assembly and operation of the smart dust sensor and therefore the photoresist patterns were used as are.

*Assembly of the smart dust sensor:* Solutions containing the to required compounds were applied as a droplet onto the sensor surface. Exchange of solutions was carried out by suction and subsequent deposition of a new droplet. The compounds were mounted in the following order: 1. casein, 2. kinesin, 3. biotinylated and

rhodamine-labeled microtubules, as tracers and 4. biotinylated fluorescein microspheres (see figure 3).

Microspheres with a diameter of 40 nm were chosen, since pick-up of bigger microspheres ( $\varnothing$  200 nm and 1  $\mu$ m) from the surface by moving microtubules was poor (see also chapter C, this report). To prevent dry-up, degradation and photobleaching during fluorescence microscopy, the sensor was kept under an atmosphere of humidified nitrogen except during solution exchange.

In contrast to casein and kinesin, which are only a few nanometers in diameter, the glass area under the pronounced SU8 is not accessible for the larger microtubules and microspheres in the diffusion based assembly process. Therefore the adsorption of microtubules and microspheres is restricted to the central area of the sensor surface.

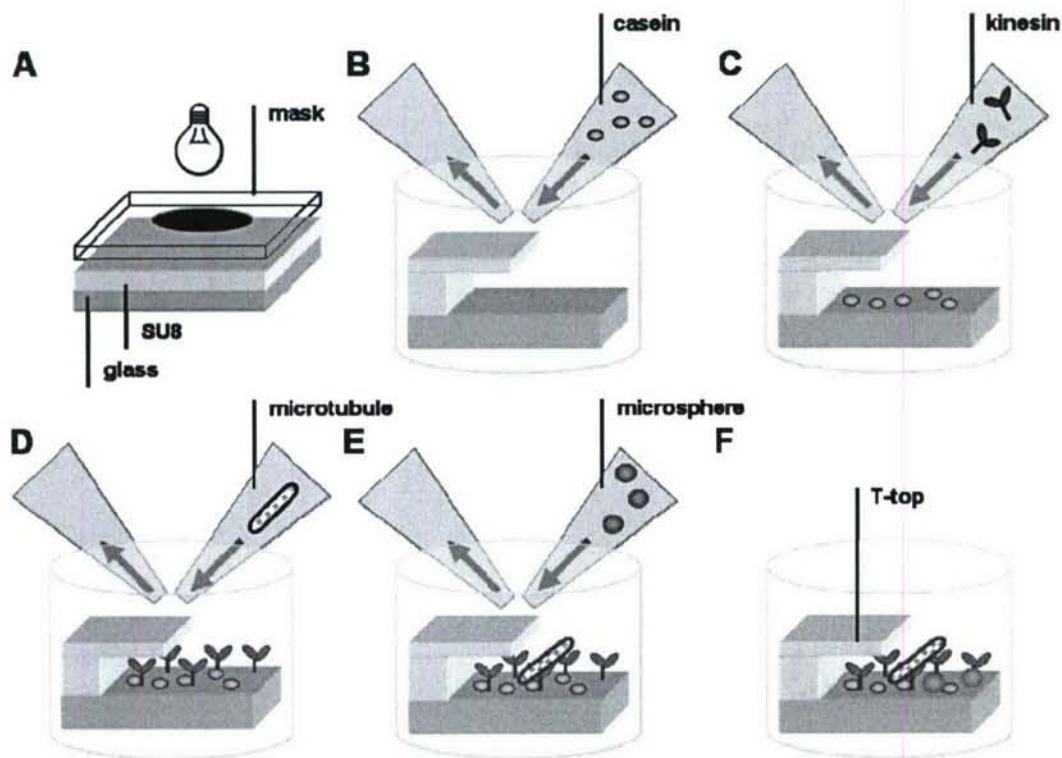


Figure 3: Key fabrication steps in the assembly of the smart dust sensor. Photolithography of SU8 on a glass substrate (A). Sequential mounting of the key components via microliter fluid exchange techniques: casein (B), kinesin (C), biotinylated microtubules (D) and biotinylated fluorescein microspheres (E). Due to the pronounced SU8 T-top the glass area under it is shielded and adsorption of microtubules and microspheres is restricted to the central area of the sensor. The fully-assembled sensor is stored under a protective droplet of aqueous buffer to prevent dry-up (F).

*Operation of the smart dust sensor:* Since no microspheres are adsorbed under the T-top, this area can be used as the detection area of the sensor. Only by microtubule transport can the fluorescent microspheres reach this area. For this to happen, the microspheres have to be picked-up from the sensor surface by the moving microtubules. Since the biotinylated microspheres show no non-specific binding to the microtubules, they will only bind in the presence of streptavidin, the analyte this smart dust sensor is specific to.

To prove this principle of operation a droplet of an alexa-fluor 568 labeled streptavidin solution was deposited on the sensor surface. During this initial step the streptavidin diffused into the sensor and bound in part to the static biotinylated microtubules and microbeads. To start microtubule movement the sensor was subsequently irradiated with UV-light to release ATP from the caged ATP containing streptavidin solution. The exposure time was 90 s and resulted in a microtubule speed of 100-200 nm/s, which is in good compliance with the optimum speed for pick-up of 40 nm microspheres (see chapter C, this report). During the movement more streptavidin bound to the microtubules (analyte harvesting). In case of contact biotinylated spheres were picked-up from the surface by binding to streptavidin which was prior bound to the biotin on the microtubules.

Furthermore spheres which were covered with bound streptavidin could be picked-up by free biotin on the microtubules (analyte tagging).

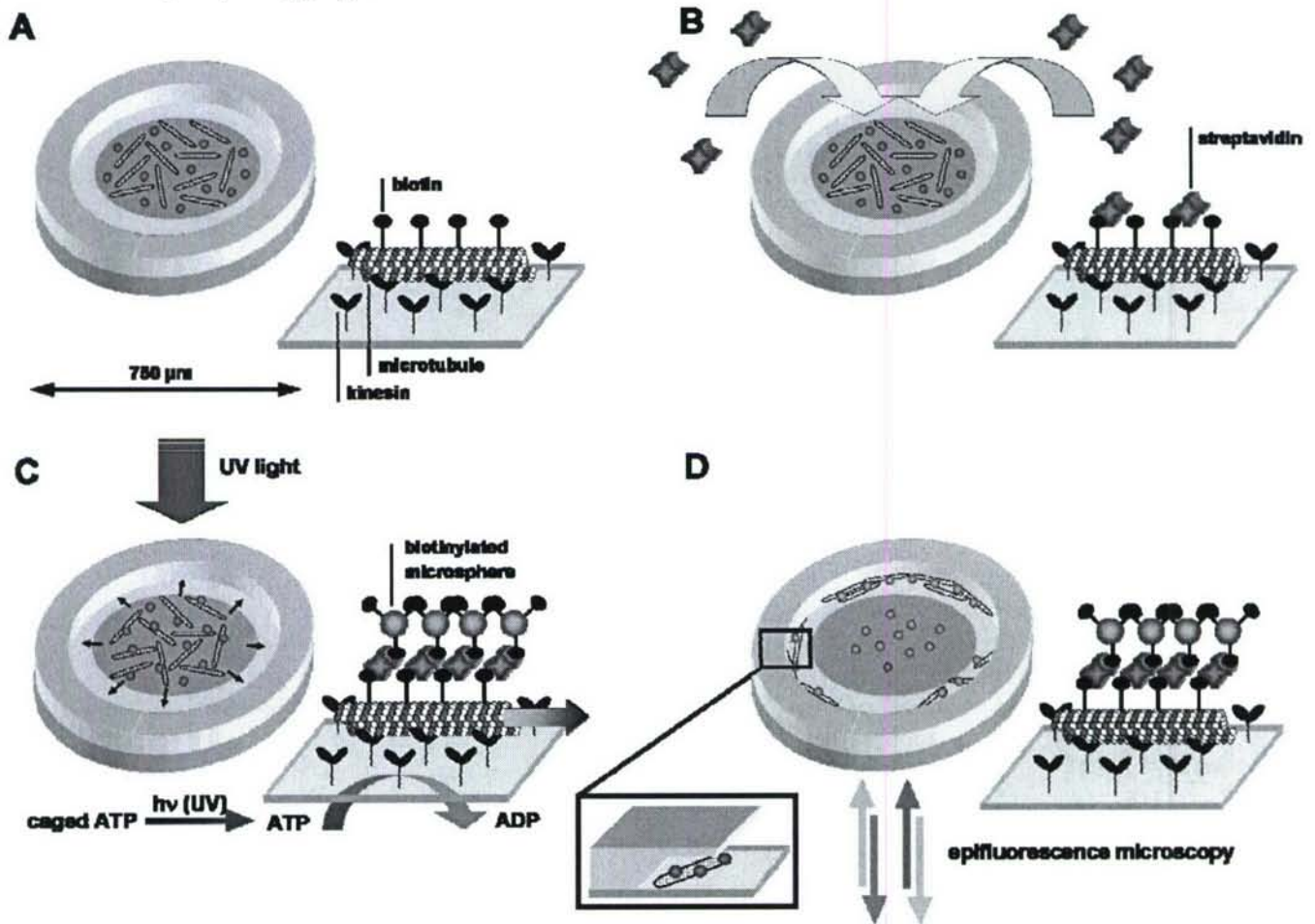


Figure 4: Mode of operation of the smart dust sensor. The protective droplet of aqueous buffer on-top of the sensor is omitted in all pictures. Due to the pronounced SU8 T-top microtubules and microbeads are spatially restricted to the central area of the sensor (dark blue circle). (A) Alexa-fluor 568 labeled streptavidin, as the analyte, diffuses into the sensor and binds in part to the static biotinylated microtubules and microbeads (not shown)(B). By irradiating the sensor with UV-light ( $E_m$  350 nm) ATP is released and the microtubules start moving over the sensor surface. More streptavidin binds to the moving microtubules (analyte harvesting) and microspheres get picked-up from the surface (analyte tagging)(C). Microtubules, which move under the SU8 T-top get stuck and stop in their movement (analyte detection area). The sensor is read-out by epifluorescence microscopy. The microspheres emit a green and the streptavidin a red fluorescence (D).

*Read-out of the smart dust sensor:* The sensor was read-out after 6 h by epifluorescence microscopy. Figure 5A shows the fluorescence of the alexa-fluor 568 labeled streptavidin bound to the microtubules/beads and the rhodamine tracer microtubules. The high intensity of fluorescence next to sensor side walls shows that the microtubules concentrated in this area during sensor operation. Imaging this area at a higher magnification reveals that the microtubules moved under the T-top, got stuck under the undercut created by the strong negative side wall slope of the SU8 resist and stopped their movement (see figure 5C and 4D). In figure 5B the fluorescence of the fluorescein-containing microspheres can be seen. The biotin-coated fluorescent beads transported via microtubules can be seen as a fluorescent ring next to the sensor's side walls. This ring is the positive read-out of the sensor showing the presence of the analyte, since otherwise no transport of microspheres to the area under the T-top would have taken place. In figure 5C both images were overlaid to give a false color image showing at a higher magnification the streptavidin-coated microtubules in red and the

microspheres in green. Clearly, the microsphere transport is mediated by the microtubules, since all beads are connected to microtubules.

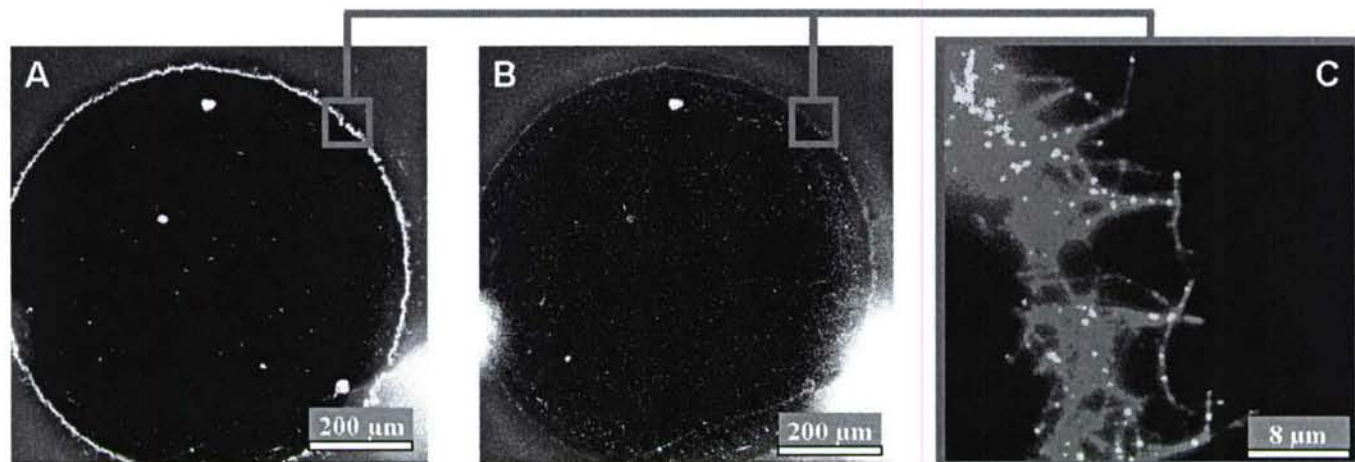


Figure 5: Epifluorescence image of a smart sensor in the analyte detection phase ( $\text{\O}$  750  $\mu\text{m}$ ). Fluorescence of alexa-fluor 568 labeled streptavidin bound to the microtubules/beads and rhodamine tracer microtubules (Ex 535 nm, Em 610 nm) (A). Fluorescence of fluorescein-containing microspheres (Ex 480 nm, Em 535 nm). The biotin-coated fluorescent beads transported via microtubules can be seen as a fluorescent ring next to the sensor's side walls (B). Both images were overlaid to give a false color image showing at a higher magnification the streptavidin-coated microtubules in red and the microspheres in green (C).

**Discussion and Conclusion:** The described single-chamber device is the first functional device powered by biomolecular motors. As such, it represents a breakthrough. Starting from this point, a functional prototype can be iteratively improved with a focus on solving actual rather than anticipated problems. The next step is to functionalize the gliding microtubules and the optical tags with antibodies and demonstrate the detection of the targeted antigen. This step is pursued now with funding from the Office of Naval Research through the University of Florida Center for Sensor Materials and Technologies. Additional future tasks include a sensitivity and selectivity analysis and the quantification of the sensor's fluorescent readout signal.

- 1 Moorjani, Samira G. , Jia, Lili , Jackson, Thomas N. , & Hancock, William O. Lithographically Patterned Channels Spatially Segregate Kinesin Motor Activity and Effectively Guide Microtubule Movements. *Nano Letters* 3 (5), 633-637 (2003).
- 2 Fischer, Thorsten & Hess, H. Materials chemistry challenges in the design of hybrid bionanodevices: Supporting protein function within artificial environments. *Journal of Materials Chemistry* 17, 943-951 (2007).
- 3 Hess, Henry et al. Molecular Shuttles Operating Undercover: A New Photolithographic Approach for the Fabrication of Structured Surfaces Supporting Directed Motility. *Nano Letters* 3 (12), 1651-1655 (2003).
- 4 Coy, D. L., Hancock, W. O., Wagenbach, M., & Howard, J. Kinesin's tail domain is an inhibitory regulator of the motor domain [see comments]. *Nat Cell Biol* 1 (5), 288-292 (1999).
- 5 Howard, J., Hunt, A. J., & Baek, S. Assay of microtubule movement driven by single kinesin molecules. *Methods Cell Biol* 39, 137-147 (1993).